A (μ-Oxo)bis(μ-carboxylato)diiron(III) Complex with a Tethered Phenoxyl Radical as a Model for the Active Site of the R2 Protein of Ribonucleotide Reductase

David P. Goldberg,[†] Dionysios Koulougliotis,[‡] Gary W. Brudvig,*[,‡] and Stephen J. Lippard*[,†]

Contribution from the Departments of Chemistry, Massachusetts Institute of Technology, Cambridge, Massachusetts 02139, and Yale University, 225 Prospect St., New Haven, Connecticut 06511

Received November 21, 1994[⊗]

Abstract: We have designed and synthesized a novel bidentate nitrogen donor ligand, 1,1-bis(2-(1-methylimidazolyl))-1-(3,5-di-*tert*-butyl-4-hydroxyphenyl)ethane (BIDPhEH) (**2**). The phenoxyl radical form of this ligand, BIDPhE (**3**), was prepared and isolated as a stable solid. BIDPhEH was used in the synthesis of the mononuclear ferric complex, $[Fe(BIDPhEH)_2Cl_2]X$ (X = Cl (**5a**), $FeCl_4$ (**5b**). The crystallographic characterization of **5b** is reported. Use of the solvento complex $[Fe_2O(XDK)(MeOH)_5(H_2O)](NO_3)_2$, where XDK is *m*-xylenediaminebis(Kemp's triacid)-imide, a pre-organized, cleft-shaped dicarboxylate ligand, facilitated preparation of the phenoxyl radical (μ-oxo)-bis(μ-carboxylato)diiron(III) complex $[Fe_2O(XDK)(BIDPhE)_2(NO_3)_2]$ (**6**), a new model for the tyrosyl radical containing active site of the R2 protein of *E. coli* ribonucleotide reductase. Magnetic susceptibility studies of **6** revealed overall magnetic behavior quite similar to that of the protein. The iron atoms are antiferromagnetically coupled, and a theoretical fit of the data determined the *J* value ($\mathcal{H} = -2JS_1 \cdot S_2$) to be -117 cm^{-1}. Pulsed saturation−recovery EPR experiments conducted on **6** provided an independent measure of *J*, the value of which was in excellent agreement with the magnetic susceptibility measurements. Comparisons are made to the saturation−recovery EPR results for the R2 protein.

Introduction

Tyrosyl radicals have been implicated in the functioning of several biological systems,[1−5] including metalloproteins such as the oxygen-evolving complex in photosystem II (PSII),[6] galactose oxidase,[7−9] prostaglandin H synthase (PGH synthase),[10] and the R2 protein of ribonucleotide reductase (RR).[11,12] The manganese-containing protein complex of PSII has two tyrosyl radicals (designated Y_Z and Y_D), one of which (Y_Z) transfers the oxidizing equivalents, necessary for the oxidative coupling of H_2O to dioxygen, to a tetranuclear manganese cluster.[6] Galactose oxidase has been proposed to utilize a Cu(II) center in conjunction with a tyrosyl radical to effect the oxidation of a broad range of alcohols to aldehydes. Recent characterization by X-ray crystallography revealed a mononuclear cupric active site with a novel cysteinyl-modified tyrosine residue bound directly to the copper atom.[13,14] This residue is almost certainly the source of a tyrosyl radical.[15] In PGH synthase, an iron porphyrin-based active site is responsible for transforming arachidonic acid to prostaglandin H_2, the first committed step in the biosynthesis of prostaglandins.[10] Spectroscopic evidence supports the involvement of a tyrosyl radical working together with the heme iron prosthetic group.[16−18] A recent 3.5 Å resolution crystallographic determination of the structure of PGH synthase reveals a tyrosine residue oriented in the active site in a manner fully consistent with a mechanism involving its conversion to the tyrosyl radical form.[19] All of these systems have in common the feature of metal-based active sites with nearby, redox-active tyrosyl residues.

Ribonucleotide reductase enzymes, of which there are three classes,[20] are essential to all living organisms, being required for the conversion of ribonucleotides to deoxyribonucleotides. The RR enzyme from *E. coli* is the best studied, belonging to the class which contains a dinuclear iron center and stable tyrosyl radical. Although reduction of the ribose ring occurs within the R1 subunit of RR from *E. coli*, the R2 subunit is

[†] Massachusetts Institute of Technology.

[‡] Yale University.

[⊗] Abstract published in *Advance ACS Abstracts*, March 1, 1995.

(1) Goldberg, D. P.; Lippard, S. J. In *Mechanistic Bioinorganic Chemistry*; Thorp, H. H., Pecoraro, V., Eds.; American Chemical Society: Washington, DC, 1995, in press.

(2) Pedersen, J. Z.; Finazzi-Agro, A. *FEBS Lett.* **1993**, *325*, 53−58.

(3) Ochiai, E.-I. *J. Chem Ed.* **1993**, *70*, 128−133.

(4) Stubbe, J. *Annu. Rev. Biochem.* **1989**, *58*, 257−285.

(5) Prince, R. C. *TIBS* **1988**, *13*, 152−154.

(6) Debus, R. J. *Biochim. Biophys. Acta* **1992**, *1102*, 269−352.

(7) Hamilton, G. A. In *Copper Proteins*; Spiro, T. G., Ed.; John Wiley & Sons, Inc.: New York, 1981; Vol. 3, pp 193−218.

(8) Ettinger, M. J.; Kosman, D. J. In *Copper Proteins*; Spiro, T. G., Ed.; John Wiley & Sons, Inc.: New York, 1981; Vol. 3, pp 219−261.

(9) Avigad, G.; Amaral, D.; Asensio, C.; Horecker, B. L. *J. Biol. Chem.* **1962**, *237*, 2736−2743.

(10) Smith, W. L.; Marnett, L. J. *Biochim. Biophys. Acta* **1991**, *1083*, 1−17.

(11) Fontecave, M.; Nordlund, P.; Eklund, H.; Reichard, P. In *Advances in Enzymology and Related Areas of Molecular Biology*; Meister, A., Ed.; John Wiley and Sons: New York, 1992; Vol. 65, pp 147−183.

(12) Stubbe, J. In *Advances in Enzymology and Related Areas of Molecular Biology*; Meister, A., Ed.; John Wiley and Sons: New York, 1990; Vol. 63, pp 349−420.

(13) Ito, N.; Phillips, S. E. V.; Yadav, K. D. S.; Knowles, P. F. *J. Mol. Biol.* **1994**, *238*, 794−814.

(14) Ito, N.; Phillips, S. E. V.; Stevens, C.; Ogel, Z. B.; McPherson, M. J.; Keen, J. N.; Yadav, K. D. S.; Knowles, P. F. *Nature* **1991**, *350*, 87−90.

(15) Babcock, G. T.; El-Deeb, M. K.; Sandusky, P. O.; Whittaker, M. M.; Whittaker, J. W. *J. Am. Chem. Soc.* **1992**, *114*, 3727−3734.

(16) Kulmacz, R. J.; Palmer, G.; Wei, C.; Tsai, A.-l. *Biochemistry* **1994**, *33*, 5428−5439.

(17) Tsai, A.-l.; Hsi, L. C.; Kulmacz, R. J.; Palmer, G.; Smith, W. L. *J. Biol. Chem.* **1994**, *269*, 5085−5091.

(18) Smith, W. L.; Eling, T. E.; Kulmacz, R. J.; Marnett, L. J.; Tsai, A.-l. *Biochemistry* **1992**, *31*, 3−7.

(19) Picot, D.; Loll, P. J.; Garavito, R. M. *Nature* **1994**, *367*, 243−249.

(20) Reichard, P. *Science* **1993**, *260*, 1773−1777.

0002-7863/95/1517-3134$09.00/0

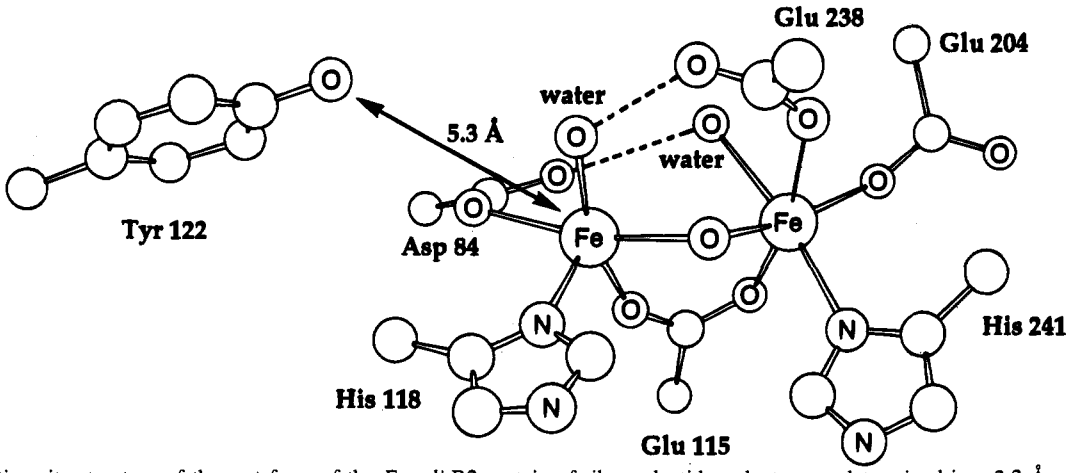

Figure 1. Active site structure of the met form of the *E. coli* R2 protein of ribonucleotide reductase as determined in a 2.2 Å resolution X-ray crystallographic study.[21,22]

responsible for generating and maintaining a stable tyrosyl radical essential to enzyme functioning. An oxo, carboxylato-bridged diiron(III) site has been structurally characterized in a crystallographic study of the R2 protein. The tyrosyl radical, Tyr122, is located in close proximity to the iron atoms, the distance from its phenolic oxygen atom to the nearest iron atom being 5.3 Å.[21,22] A diagram of the active site of the R2 subunit is given in Figure 1.

A molecular mimic of the R2 active site must incorporate at least two important features, a (μ-oxo)(μ-carboxylato)diiron-(III) core and a stable phenoxyl radical held close, but not coordinated, to the diferric center. Previous work in our laboratory has afforded synthetic methodology for accessing $[Fe_2X(O_2CR)_2L_2]^{n+}$ complexes, X = O or OH, which have accurately modeled the structural and spectroscopic properties of the non-heme iron centers in metalloproteins such as ribonucleotide reductase, hemerythrin, methane monooxygenase, and purple acid phosphatase.[23-30] In these complexes, L can be one of various bidentate or tridentate nitrogen donor ligands. This experience suggested that it should be possible to design a nitrogen donor ligand L containing a stable phenoxyl radical in close proximity, but not coordinated, to the $[Fe_2O(O_2CR)_2]^{2+}$ core.

Although other phenoxyl radical metal complexes have been reported,[31-36] they were not designed to prevent delocalization of the radical spin to the metal center. Moreover, most were only generated in situ and characterized by EPR spectroscopy, and very few were isolated as solids. A recent specific attempt to model metalloenzymes containing tyrosyl radicals afforded two related tris(phenolato)iron(III) complexes which could be oxidized to the $[Fe(L)]^{\bullet+}$ radical cations, one of which was isolated as a stable powder.[37] In these species the oxidizing equivalent is localized on one of the phenolate donors to give a phenoxyl radical which is coordinated directly to the Fe(III) atom through its oxygen atom.[37] A related report describes the synthesis of a series of sulfur-substituted phenols and their corresponding phenoxyl radicals as models for galactose oxidase.[38]

In the present work we describe the synthesis of the novel bidentate nitrogen donor ligand 1,1-bis-(2-(1-methylimidazolyl))-1-(3,5-di-*tert*-butyl-4-hydroxyphenyl)ethane (BIDPhEH), which contains biomimetic imidazole donors and a redox-active pendant phenol group. This ligand is closely related to BIPhMe, which was successfully employed in the synthesis of (μ-oxo)-bis(μ-carboxylato)diiron(III) complexes.[28,29] A method has been

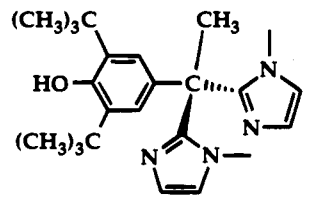

BIDPhEH

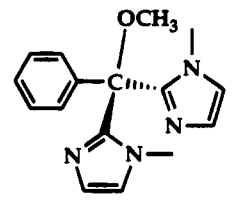

BIPhMe

developed for oxidizing BIDPhEH to the phenoxyl radical form BIDPhE, which was employed as a ligand in the synthesis of a (μ-oxo)bis(μ-carboxylato)diiron(III) complex with two pendant phenoxyl radical capping ligands. This model of the R2 active site was isolated and characterized as a stable crystalline solid. The synthesis and structure of a mononuclear BIDPhEH complex of iron(III) are also reported, providing structural information about the coordination of BIDPhE(H) to ferric ion. The phenoxyl radical diiron(III) model complex was probed by

(21) Nordlund, P.; Eklund, H. *J. Mol. Biol.* **1993**, *232*, 123–164.
(22) Nordlund, P.; Sjöberg, B.-M.; Eklund, H. *Nature* **1990**, *345*, 593–598.
(23) Armstrong, W. H.; Spool, A.; Papaefthymiou, G. C.; Frankel, R. B.; Lippard, S. J. *J. Am. Chem. Soc.* **1984**, *106*, 3653–3667.
(24) Lippard, S. J. *Angew. Chem., Int. Ed. Engl.* **1988**, *27*, 344–361.
(25) Beer, R. H.; Tolman, W. B.; Bott, S. G.; Lippard, S. J. *Inorg. Chem.* **1989**, *28*, 4557–4559.
(26) Turowski, P. N.; Armstrong, W. H.; Roth, M. E.; Lippard, S. J. *J. Am. Chem. Soc.* **1990**, *112*, 681–690.
(27) Beer, R. H.; Tolman, W. B.; Bott, S. G.; Lippard, S. J. *Inorg. Chem.* **1991**, *30*, 2082–2092.
(28) Tolman, W. B.; Liu, S.; Bentsen, J. G.; Lippard, S. J. *J. Am. Chem. Soc.* **1991**, *113*, 152–164.
(29) Taft, K. L.; Masschelein, A.; Liu, S.; Lippard, S. J.; Garfinkel-Shweky, D.; Bino, A. *Inorg. Chim. Acta* **1992**, *198*–200, 627–631.
(30) Watton, S. P.; Masschelein, A.; Rebek, J., Jr.; Lippard, S. J. *J. Am. Chem. Soc.* **1994**, *116*, 5196–5205.
(31) Kompan, O. E.; Ivakhnenko, E. P.; Lyubchenko, S. N.; Olekhnovich, L. P.; Yanovskii, A. I.; Struchkov, Y. T. *J. Gen. Chem. USSR (Engl. Transl.)* **1990**, 1682–1690.
(32) Ivakhnenko, E. P.; Lyubchenko, S. N.; Kogan, V. A.; Olekhnovich, L. P.; Prokof'ev, A. I. *J. Gen. Chem. USSR (Engl. Transl.)* **1986**, *56*, 765–768.
(33) Melezhik, A. V.; Vovk, D. N.; Pokhodenko, V. D. *J. Gen. Chem. USSR (Engl. Transl.)* **1983**, *53*, 1442–1447.
(34) Melezhik, A. V.; Pokhodenko, V. D. *J. Org. Chem. USSR (Engl. Transl.)* **1982**, *18*, 912–917.
(35) Pokhodenko, V. D.; Melezhik, A. V.; Vovk, D. N. *Sov. J. Coord. Chem. (Engl. Transl.)* **1982**, *8*, 667–671.
(36) Shultz, D. A.; Knox, D. A.; Morgan, L. W.; Sandberg, K.; Tew, G. N. *Tetrahedron Lett.* **1993**, *34*, 3975–3978.
(37) Hockertz, J.; Steenken, S.; Wieghardt, K.; Hildebrandt, P. *J. Am. Chem. Soc.* **1993**, *115*, 11222–11230.
(38) Whittaker, M. M.; Chuang, Y.-Y.; Whittaker, J. W. *J. Am. Chem. Soc.* **1993**, *115*, 10029–10035.

magnetic susceptibility and X-band EPR saturation−recovery experiments. Aspects of this work have appeared in preliminary form.[39]

Experimental Section

Materials and General Methods. Unless otherwise noted, materials were obtained from commercial sources and used as received. Where appropriate, manipulations and reactions were carried out under an inert atmosphere in a Vacuum Atmospheres drybox or by using standard Schlenk techniques. Solvents THF, C_6H_6, and pentane were distilled from Na/benzophenone ketyl under nitrogen; CH_2Cl_2 was distilled from CaH_2 under nitrogen. All other solvents were purchased as reagent grade and used as received. 1-Methylimidazole, *n*-butyllithium, and methyllithium were purchased and used as received. Methyl 3,5-di-*tert*-butyl-4-hydroxybenzoate was prepared in 96% yield by esterification from the corresponding benzoic acid, which was purchased from Aldrich and used as received. $[Fe_2O(XDK)(MeOH)_5(H_2O)](NO_3)_2 \cdot 4H_2O$ and the ligand H_2XDK (XDK = xylenediaminebis(Kemp's triacid)-imide) were prepared according to literature procedures.[30] [Zn(BIDPhE)Cl_2] was prepared as described elsewhere.[39] A standard solution of $Na_2S_2O_3$ was purchased from J. T. Baker Co. ^1H and ^{13}C NMR spectra were recorded on a Bruker AC250 or Varian XL300 spectrometer. Proton resonances, reported in units of ppm downfield from tetramethylsilane (TMS), were referenced to residual solvent protons. Mass spectra were obtained on a Finnigan MAT 8200 mass spectrometer. Melting points are uncorrected.

Bis(1-methylimidazolyl)(3,5-di-*tert*-butyl-4-hydroxyphenyl)hydroxymethane (1). A solution containing 39.8 mL (0.499 mol) of 1-methylimidazole dissolved in 400 mL of freshly distilled THF was cooled to −78 °C under argon, and a 2.5 M solution of *n*-butyllithium in hexanes (200 mL, 0.500 mol) was added dropwise. A solution of methyl 3,5-di-*tert*-butyl-4-hydroxybenzoate (44.0 g, 0.170 mmol) in THF was added to the reaction mixture. The solution was stirred for 1 h at −78 °C and allowed to warm to room temperature, during which time a large amount of white solid precipitated. The heterogeneous mixture was stirred for an additional 12 h, at which point H_2O was added to quench any excess base remaining and dissolve the white precipitate. The pH was brought close to 7 with aqueous HCl, and the THF and aqueous phases were separated. In some preparations the product crystallized directly from the THF layer upon standing, in which case the crystals were isolated, washed with ice-cold diethyl ether, and used directly in the next step. The aqueous phase was extracted with CH_2Cl_2, and the extracts were washed with brine. All organic layers were combined and dried over $MgSO_4$. The organic phase was filtered and the solvents were removed under vacuum to give an orange solid. The product was purified by recrystallization from C_6H_6, followed by washing with ice-cold diethyl ether, to give 39.5 g (59%) of a white powder. Mp 166−167.5 °C; ^1H NMR ($CDCl_3$, 250 MHz) δ 6.93 (d, J = 1 Hz, Im, 2H), 6.86 (d, J = 1 Hz, Im, 2H), 6.82 (s, phenyl, 2H), 6.43 (s, OH, 1H), 5.26 (s, PhOH, 1H), 3.38 (s, MeIm, 6H), 1.34 (s, *t*-Bu, 18H); ^{13}C {^1H} NMR (acetone-d_6, 250 MHz) δ 154.5, 150.0, 137.8, 134.2, 126.0, 124.9, 124.2, 75.9, 35.1, 34.8, 30.6; FAB-MS *m/e* (relative intensity): calcd *m/e* for $(M + H)^+$ 397.3; found 397.4 ($(M + H)^+$, 28), 380.4 (−OH, 8), 315.3 (−MeIm, 10).

1,1-Bis(2-(1-methylimidazolyl))-1-(3,5-di-*tert*-butyl-4-hydroxyphenyl)ethane (BIDPhEH) (2). A solution of **1** (11.98 g, 30.2 mmol) in THF was cooled to −78 °C under argon, and a 1.6 M solution of CH_3Li in Et_2O (18.9 mL, 30.2 mmol) was added dropwise. The reaction mixture was stirred for 2 h at −78 °C and warmed to room temperature to give a slurry, which was refluxed for 48 h to afford a bright orange reaction mixture containing the quinone methide intermediate. This species was identified by comparison of its ^1H NMR spectrum with that of an authentic sample (vide infra). This solution was cooled to −78 °C, and a 1.6 M solution of CH_3Li in Et_2O (37.8 mL, 48.0 mmol) was added by syringe, causing a color change from orange to red-brown. After 1 h, the reaction mixture was allowed to warm to room temperature and stirred for an additional 12 h.

The reaction mixture was quenched with H_2O and the pH was adjusted to 7 with the addition of aqueous HCl. The THF/H_2O mixture was extracted with CH_2Cl_2 and the combined organic layers were washed with a saturated $NaHCO_3$ solution, then brine, and dried over $MgSO_4$. The organic layer was filtered and evaporated to give 9.50 g of crude product. The product was purified by recrystallization from acetone followed by careful washing with ice-cold acetone and Et_2O, affording 4.39 g (37%) of a white powder. Mp 184.5−185.0 °C; ^1H NMR ($CDCl_3$, 250 MHz) δ 6.98 (d, J = 1 Hz, Im, 2H), 6.85 (s, phenyl, 2H), 6.82 (d, J = 1 Hz, Im, 2H), 5.11 (s, OH, 1H), 3.10 (s, MeIm, 6H), 2.19 (s, CH_3, 3H), 1.34 (s, *t*-Bu, 18H); ^{13}C {^1H} NMR ($CDCl_3$, 300 MHz) δ 152.3, 149.8, 134.8, 133.9, 126.4, 124.6, 122.6, 47.0, 34.2, 33.8, 30.3, 29.1; EI-MS *m/e* (relative intensity) 394 (M^+, 100), 379 (42), 352 (21), 310 (28), 189 (19), 176 (22), 175 (30), 83 (19), 57 (18). Anal. Calcd for $C_{24}H_{34}N_4O$: C, 73.06, H, 8.69; N, 14.20. Found: C, 73.58; H, 8.80; N, 14.53.

1,1-Bis(2-(1-methylimidazolyl))-1-(3,5-di-*tert*-butyl-4-oxylphenyl)ethane (BIDPhE) (3). The phenol **2** (0.500 g, 1.27 mmol) was dissolved in 20.0 mL of distilled, degassed C_6H_6 in a 100 mL Schlenk flask under argon. A solution of $K_3Fe(CN)_6$ (2.0 g, 6.07 mmol) and NaOH (1.2 g, 30.0 mmol) was prepared by dissolving the solids in 20.0 mL of H_2O and purging with argon for 15−30 min. This solution was transferred to the solution of **2**, and an immediate deep blue color was formed in the organic layer. The two-phase reaction mixture was stirred for 1.0 h, at which point the aqueous phase was removed. The C_6H_6 layer was washed with 2 × 10 mL portions of degassed H_2O and then transferred to a 50 mL Schlenk flask containing $MgSO_4$. After 0.5 h, the C_6H_6 layer was filtered and the solvent removed by vacuum over a 2−3 h period at ambient temperature to yield 0.440 g (88%) of **2** as a dark green solid. Electronic spectral data in CH_3CN solution (λ_{max}, nm (ϵ, M^{-1} cm^{-1})): 638 (430), 394 (1700), 378 (1500). The purity of the radical **2** was qualitatively established by TLC (silica gel, CH_3CN/Et_2O 80/20, r_f = 0.3) and quantitated (94%) by iodometric titration.[40]

2,6-Di-*tert*-butyl-4-(bis[2-(1-methylimidazolyl)]methyl))-2,5-cyclohexadienone (4). To a solution of **1** (1.02 g, 2.57 mmol) in THF (50 mL), cooled to −78 °C, was added a 1.6 M solution of *n*-BuLi in hexanes (1 mL, 2.5 mmol), dropwise by syringe, giving a green precipitate. The mixture was warmed to room temperature and stirred for 12 h. A yellow precipitate was observed and the mixture was refluxed for 1 day to give a red-orange solution. The THF solvent was evaporated and the resulting orange solid was dissolved in CH_2Cl_2 and filtered through a Celite plug. Removal of the CH_2Cl_2 under vacuum afforded 0.874 g (87%) of an orange powder. Mp 201.5−204.5 °C; ^1H NMR (acetone-d_6, 250 MHz) δ 7.65 (s, phenyl, 2H), 7.33 (d, J = 1 Hz, Im, 2H), 7.22 (d, J = 1 Hz, Im, 2H), 3.14 (s, MeIm, 6H), 1.24 (s, *t*-Bu, 18H); ^{13}C {^1H} NMR ($CDCl_3$, 300 MHz) δ 186.5, 149.1, 144.5, 136.1, 130.6, 130.2, 126.0, 123.8, 35.3, 33.1, 29.4. Anal. Calcd for $C_{23}H_{30}N_4O$: C, 72.98; H, 7.99; N, 14.80. Found: C, 72.86; H, 8.00; N, 14.84.

[Fe(BIDPhEH)$_2$Cl$_2$]Cl · H$_2$O (5a · H$_2$O). An amount of $FeCl_3$ (0.083 g, 0.512 mmol) was combined with BIDPhEH (0.405 g, 1.05 mmol) in CH_3CN (10 mL) to give a red-orange solution. After 1 h, the reaction mixture was filtered, and subsequent vapor diffusion of Et_2O afforded **5a** as red crystals. The supernatant was decanted, and the crystals were washed with Et_2O, crushed, and dried under vacuum at 111 °C for 12 h, affording 0.487 g (52%) of an orange powder. FTIR (KBr pellet): 3131, 2958, 1556, 1482, 1436, 1395, 1366, 1335, 1280, 1230, 1204, 1157, 1136, 1097, 1076, 953, 890, 813, 775, 732, 709, 666, 549, 538, 482 cm^{-1}. Anal. Calcd for $FeC_{48}H_{70}Cl_3N_8O_3$ (**5a** · H_2O): C, 59.48; H, 7.28; N, 11.56. Found: C, 59.48; H, 7.13; N, 11.51. Three analyses of independent samples of **5a** gave satisfactory results for **5a** · H_2O, with or without heating under vacuum.

[FeL$_2$Cl$_2$][FeCl$_4$] · CH$_3$CN (5b · CH$_3$CN). An amount of $FeCl_3$ (0.045 g, 0.277) was combined with BIDPhEH (0.110 g, 0.279 mmol) in CH_3CN (5 mL) to give an orange-brown solution. After 24 h, the reaction mixture was filtered, and subsequent vapor diffusion of Et_2O afforded **5b** as orange crystals. FTIR (KBr pellet) 3615, 3566, 3142, 2961, 2873, 1553, 1483, 1434, 1366, 1335, 1281, 1239, 1208, 1135, 953, 892, 811, 758, 731, 705, 536, 481 cm^{-1}. Anal. Calcd for $Fe_2C_{50}H_{71}Cl_6N_9O_2$ (**5b** · CH_3CN): C, 52.01; H, 6.20; N, 10.92. Found: C, 51.74; H, 6.23; N, 10.71.

(39) Goldberg, D. P.; Watton, S. P.; Masschelein, A.; Wimmer, L.; Lippard, S. J. *J. Am. Chem. Soc.* **1993**, *115*, 5346−5347.

(40) Bartlett, P. D.; Funahashi, T. *J. Am. Chem. Soc.* **1962**, *84*, 2596−2601.

$[Fe_2O(XDK)(BIDPhE)_2(NO_3)_2] \cdot CH_2Cl_2$ ($6 \cdot CH_2Cl_2$). All manipulations were carried out in a drybox. A portion of $[Fe_2O(XDK)(MeOH)_5(H_2O)](NO_3)_2 \cdot 4H_2O$ (0.075 g, 0.069 mmol) was added to a deep green solution of BIDPhE (**3**) (0.057 g, 0.145 mmol) in CH_2Cl_2 (3 mL) to give a dark brown-green reaction mixture. This mixture was stirred for 10 min and filtered to remove a small amount of a brown precipitate. Pentane was added dropwise to the filtrate until a small amount of brown powder was formed, and subsequent vapor diffusion of pentane into the solution at −30 to −40 °C afforded a dark brown-green crystalline material. The crystals were isolated by decanting the mother liquor and washed with pentane. The pentane washings showed no blue-green color, indicating that any uncoordinated **3** was removed with the mother liquor; **3** is readily soluble in pentane. Drying the product under vacuum for 15 min gave 0.110 g (72%) of a dark brown-green crystalline solid. FTIR (KBr pellet): 2972, 2929, 2871, 2367, 2329, 1737, 1695, 1542, 1492, 1461, 1387, 1363, 1334, 1285, 1192, 1146, 1091, 958, 887, 812, 760, 712, 640 cm^{-1}. Anal. Calcd for $Fe_2C_{81}H_{106}N_{12}Cl_2O_{17}$ ($6 \cdot CH_2Cl_2$): C, 57.15; H, 6.28; N, 9.87. Found: C, 57.52; H, 6.20; N, 9.83. The occurrence of CH_2Cl_2 in the lattice was confirmed by the ^1H NMR spectrum of $6 \cdot CH_2Cl_2$ in $CDCl_3$. The radical content of **6** was determined by measuring the absorbance of the band found at 644 nm for solutions of **6** in CH_2Cl_2, and taking the extinction coefficient for this band to be $\epsilon = 430\ M^{-1}\ cm^{-1}$, the value of the 638 nm band in compound **3**. The radical content was typically between 85 and 95% for a given batch of **6** as measured by this assay.

Iodometric Titration of Radical Content. Chemical titration was chosen as the most accurate method for determining the radical content in **3**, and a procedure was developed based on the oxidation of I^- to I_2/I_3^-. The amount of iodine generated in situ was quantitated with a standard aqueous solution of $Na_2S_2O_3$. This assay follows a method used for the phenoxyl radical galvinoxyl.[40]

One gram of NaI was dissolved in a previously degassed CH_3CO_2H/C_6H_6 (5/4 v/v, 45 mL) mixture. The appearance of any trace yellow color was an indication of the presence of I_2/I_3^-, which was taken as evidence that there was O_2 contamination in the system, in which case a fresh NaI solution was prepared. A known amount of **3** (typically ≈50 mg) was added as a solid directly to the NaI solution, and formation of the yellow-brown color of I_2/I_3^- was observed. H_2O (degassed, 20 mL per 45 mL of CH_3CO_2H/C_6H_6 solution) was added to give a 2-phase mixture. The iodine formed in situ was then titrated with a 0.01 M standard solution of $Na_2S_2O_3$. Titrations were conducted until at least three consecutive values agreed to within 5% of each other.

The reliability and accuracy of the titration procedure were tested by using galvinoxyl as a standard. The radical content obtained by the above titration method for galvinoxyl was compared to that calculated from UV−visible spectra by using the known extinction coefficient, $\epsilon = 607\ M^{-1}\ cm^{-1}$ ($\lambda_{max} = 767$ nm), for galvinoxyl.[40] The chemical titrations and UV−visible assays of the radical content in galvinoxyl agreed to within 2%.

Crystallography. An X-ray diffraction study of $[FeL_2Cl_2][FeCl_4] \cdot CH_3CN$ ($5b \cdot CH_3CN$) was performed with an Enraf-Nonius CAD-4F kappa geometry diffractometer and graphite monochromatized Mo $K_{\bar{\alpha}}$ radiation $\lambda = 0.71069$ Å. The crystal temperature (see Table 1) was maintained by the use of an Enraf-Nonius FR558-S liquid nitrogen cryostat. All calculations were performed with a VAXstation 4000-90 computer and the teXsan software package.[41] A diamond-shaped orange crystal (0.20 × 0.10 × 0.25 mm) grown from CH_3CN/Et_2O was mounted on the end of a quartz fiber with silicone grease. The unit cell dimensions were obtained from a least-squares fit of 25 reflections in the range $8° < \theta < 15°$ and revealed the Laue symmetry to be $2/m$, which was confirmed by the examination of axial photographs. The computer program TRACER[42] was employed to provide additional confirmation of the choice of crystal system. The crystal was determined to be of sufficient quality for data collection as judged by the examination of rotation and axial photographs, the unit cell parameter errors, and the measurement of selected low angle peak widths at half-height ($\Delta\bar{\omega}_{1/2}$) by open-counter ω scans.

(41) *Single Crystal Structure Analysis Software*, Version 1.6, Molecular Structure Corporation: The Woodlands, TX, 1993.

(42) Lawton, S. L. TRACER II, *A Fortran Transformation-Cell Reduction Program*; Mobil Oil Corporation: Paulsboro, NJ, 1967.

Table 1. Crystallographic Data for $[Fe(BIDPhEH)_2Cl_2][FeCl_4] \cdot CH_3CN$ ($5b \cdot CH_3CN$)

chemical formula	$Fe_2C_{50}H_{71}N_9Cl_6O_4$
formula weight	1154.58
space group	*Pbca*
a (Å)	19.984(8)
b (Å)	19.275(6)
c (Å)	29.779(14)
V (Å^3)	11471(8)
Z	8
d(calcd), (g cm^{-3})	1.34
μ, cm^{-1}	8.30
range of 2θ (deg)	3−50
octant collected	$+h+k+l$
trans coeff	0.905−1.000
no. of unique data	10940
data with $F_o^2 > 3\sigma(F_o^2)$	4742
R_{merge} (%)	2.2
no. of variables	607
$R(F_o)^a$	0.048
$R_w(F_o)^b$	0.057
goodness of fit	1.52
λ (Å)	0.71069
temp (°C)	−72

$^a R = \Sigma||F_o| - |F_c||/\Sigma|F_o|$. $^b R_w = [(\Sigma\omega(|F_o| - |F_c|/\Sigma\omega|F_o|^2]^{1/2}$; $w = 1/\sigma^2(F_o)$.

Intensity data were collected with the ω scan technique. The intensities of three standard reflections were measured every 3600 s of exposure time. The data were corrected for Lorentz and polarization effects. No decay correction was necessary during data collection since there was no significant fluctuation in the intensities of the three standard reflections. An absorption correction was applied following the measurement of psi scans.[43] The direct methods program SHELXS-86[44] was used for the initial structure solution, and final models were obtained by least-squares refinement in combination with difference Fourier syntheses. All non-hydrogen atoms were refined by using anisotropic thermal parameters, except for the lattice solvent composed of N(9), C(71), and C(72). Hydrogen atoms were placed at calculated positions (C−H = 0.95 Å), and their B values were fixed at 1.2 times the B_{eq} of the atom to which they were bound. They were included, but not refined, in the final least-squares cycles. Scattering factors for the non-hydrogen[45] and hydrogen atoms[46] and anomalous dispersion terms[47,48] were taken from the usual sources. The largest positive peak in the final difference Fourier map had an electron density of 0.47 e$^-$/Å^3 and was located in the region near C(50).

A summary of crystallographic data for **5b** can be found in Table 1. Selected bond distances and angles are given in Table 2. Atomic coordinates and B_{eq} values are given in Table S1. Complete listings of intramolecular bond distances and angles are given in Tables S2 and S3, respectively. Anisotropic thermal parameters are given in Table S4. An ORTEP diagram of the cation of **5b** is shown in Figure 2.

Physical Measurements. Magnetic Susceptibility Studies. Solid state magnetic susceptibility measurements on ≈50 mg of $6 \cdot CH_2Cl_2$ were made by using a Quantum Design MPMS SQUID susceptometer equipped with a 5.5 T magnet. Samples were loaded in a drybox and sealed in nitrogen-filled vials for transport to the susceptometer. The susceptibilities of the sample holder were measured at the same fields and temperatures for accurate corrections of its contribution to the total measured susceptibility. A diamagnetic correction of -664×10^{-6} was estimated from Pascal's constants[49,50] and subtracted from the experimental susceptibilities.

(43) North, A. C. T.; Phillips, D. C.; Mathews, F. S. *Acta Crystallogr.* **1968**, *A24*, 351−359.

(44) Sheldrick, G. M. *SHELXS86. Program for crystal structure determination;* University of Göttingen: Göttingen, 1986.

(45) Cromer, D. T.; Waber, J. T. In *International Tables for X-ray Crystallography;* Kynoch Press: Birminghani, 1974; Vol. 4, pp 71−98.

(46) Stewart, R. F.; Davidson, E. R.; Simpson, W. T. *J. Chem. Phys.* **1965**, *42*, 3175−3187.

(47) Ibers, J. A.; Hamilton, W. C. *Acta Crystallogr.* **1964**, *17*, 781.

(48) Creagh, D. C.; McAuley, W. J. In *International Tables for X-ray Crystallography;* Kluwer Academic Publishers: Dordrecht, 1992; Vol. C, pp 219−222.

(49) Carlin, R. L. *Magnetochemistry*; Springer-Verlag: New York, 1986.

Table 2. Selected Interatomic Distances (Å) and Angles (deg) for $[Fe(BIDPhEH)_2Cl_2][FeCl_4] \cdot CH_3CN$ (**5b** · CH_3CN)[a]

	(a) Distances		
Fe(1)−Cl(1)	2.317(2)	Fe(2)−Cl(3)	2.190(2)
Fe(1)−Cl(2)	2.325(2)	Fe(2)−Cl(4)	2.195(3)
Fe(1)−N(1)	2.103(5)	Fe(2)−Cl(5)	2.200(2)
Fe(1)−N(3)	2.143(5)	Fe(2)−Cl(6)	2.174(3)
Fe(1)−N(5)	2.109(5)	Fe(1)···1)	8.863(5)
Fe(1)−N(7)	2.142(5)	Fe(2)···O(2)	8.725(5)
	(b) Angles		
Cl(1)−Fe(1)−Cl(2)	93.76(7)	Cl(2)−Fe(1)−N(7)	175.1(1)
Cl(1)−Fe(1)−N(1)	94.7(1)	N(1)−Fe(1)−N(3)	81.9(2)
Cl(1)−Fe(1)−N(3)	174.6(1)	N(1)−Fe(1)−N(5)	169.5(2)
Cl(1)−Fe(1)−N(5)	91.9(1)	N(1)−Fe(1)−N(7)	89.3(2)
Cl(1)−Fe(1)−N(7)	90.3(1)	N(3)−Fe(1)−N(5)	90.9(2)
Cl(2)−Fe(1)−N(1)	93.1(1)	N(3)−Fe(1)−N(7)	85.5(2)
Cl(2)−Fe(1)−N(3)	90.6(1)	N(5)−Fe(1)−N(7)	82.5(2)
Cl(2)−Fe(1)−N(5)	94.6(1)		

[a] For atom-labeling scheme, see Figure 2. Estimated standard deviations in the least significant digits are given in parentheses.

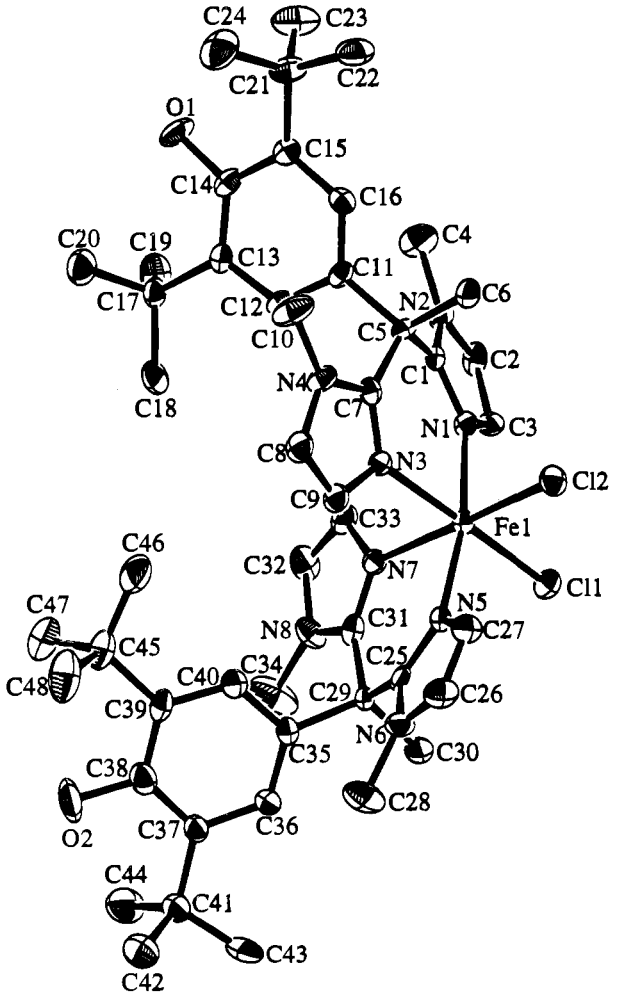

Figure 2. ORTEP diagram of the cation of $[Fe(BIDPhEH)_2Cl_2][FeCl_4] \cdot CH_3CN$ (**5b** · CH_3CN). Thermal ellipsoids are drawn at the 50% probability level. Hydrogen atoms have been omitted for clarity.

EPR Studies. Saturation−recovery and continuous wave EPR experiments were performed on a home-built X-band pulsed EPR spectrometer.[51] The magnetic field was set at the zero-crossing point of the first derivative spectrum of the phenoxyl radical (see Figure 3), that is, at the maximum of the corresponding absorption signal.

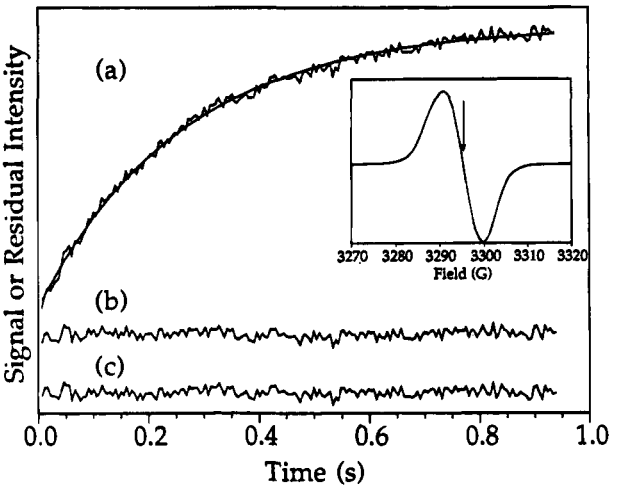

Figure 3. (a) Saturation−recovery EPR transient obtained for the BIDPhE radical in the $[Zn(BIDPhE)Cl_2]$ compound (radical concentration 0.1 mM) at 9.0 K with a single-exponential fit superimposed. The observing microwave power was 0.18 μW, the saturating microwave power was 144 mW, and the pulse was of 140 ms duration. (b) Residual difference between the experimental data and the fitted curve for the single-exponential fit. (c) Residual for the dipolar-model fit (eqs 2−3). Inset: Continuous-wave, X-band first derivative EPR spectrum of the BIDPhE radical in the $[Zn(BIDPhE)Cl_2]$ compound. The arrow points at the zero-crossing point, used as the field position setting in the saturation−recovery experiment. Experimental conditions for the CW spectrum were the following: temperature 10 K; microwave frequency, 9.07 GHz; field-modulation amplitude, 4.0 G; microwave power, 0.45 μW; field-modulation frequency, 100 kHz.

Temperature control was achieved with an Oxford ESR 900 liquid helium cryostat and calibrated by using a Si-diode sensor at the sample position. At any given temperature, three to four saturation−recovery EPR transients were recorded at different levels of observing microwave power in order to determine T_1^{-1} or $k_{1scalar}$ by linear extrapolation to zero power.[51] A nonlinear regression program written by Dr. D. Hirsh, employing the Marquardt algorithm,[52] was used to obtain fits to the saturation−recovery EPR traces. The radical concentration was ≈0.1 mM in the $[Zn(BIDPhE)Cl_2]$ compound and either ≈0.2 mM or ≈2.0 mM in compound **6**. All samples were prepared in an anaerobic CH_2Cl_2/THF (3/1 v/v) solution so as to assure the formation of a good glass upon freezing.

Results and Discussion

Syntheses. The preparation of the BIDPhEH ligand was accomplished in three steps from methyl 3,5-di-*tert*-butyl-4-hydroxybenzoate, as shown in Scheme 1. Addition of the ester to a solution of 3 equiv of the 1-methylimidazolate anion in THF afforded alcohol **1** in good yield. The target phenol BIDPhEH (**2**) was synthesized in two steps via the formation of the quinone methide intermediate **4**. Addition of 1 equiv of CH_3Li to a solution of **1** in THF, followed by refluxing, led to the formal dehydration of **1**, generating **4** in situ. Although **4** can be prepared independently from **1** by the addition of *n*-butyllithium, we found it unnecessary to isolate **4** in the synthesis of **2** since the conversion of **1** to **4** in situ is nearly quantitative. The addition of nucleophiles to quinone methides is well-known, including the use of carbanions to give the 1,6-addition product.[53,54] Addition of 2 equivs more of CH_3Li to the reaction mixture, one of which served as a sacrificial equivalent of base, afforded **2** in typical yields of 40% after purification by crystallization.

(50) O'Connor, C. J. *Prog. Inorg. Chem.* **1982**, *29*, 203−283.
(51) Beck, W. F.; Innes, J. B.; Lynch, J. B.; Brudvig, G. W. *J. Magn. Reson.* **1991**, *91*, 12−29.
(52) Press, W. H.; Flannery, B. P.; Teukolsky, S. A.; Vetterling, W. T. *Numerical Recipes in Pascal*; Cambridge University Press: Cambridge, 1989.
(53) Becker, H.-D. *J. Org. Chem.* **1967**, *32*, 4093−4095.
(54) Turner, A. B. *Q. Rev., Chem. Soc.* **1964**, *18*, 347−360.

Scheme 1

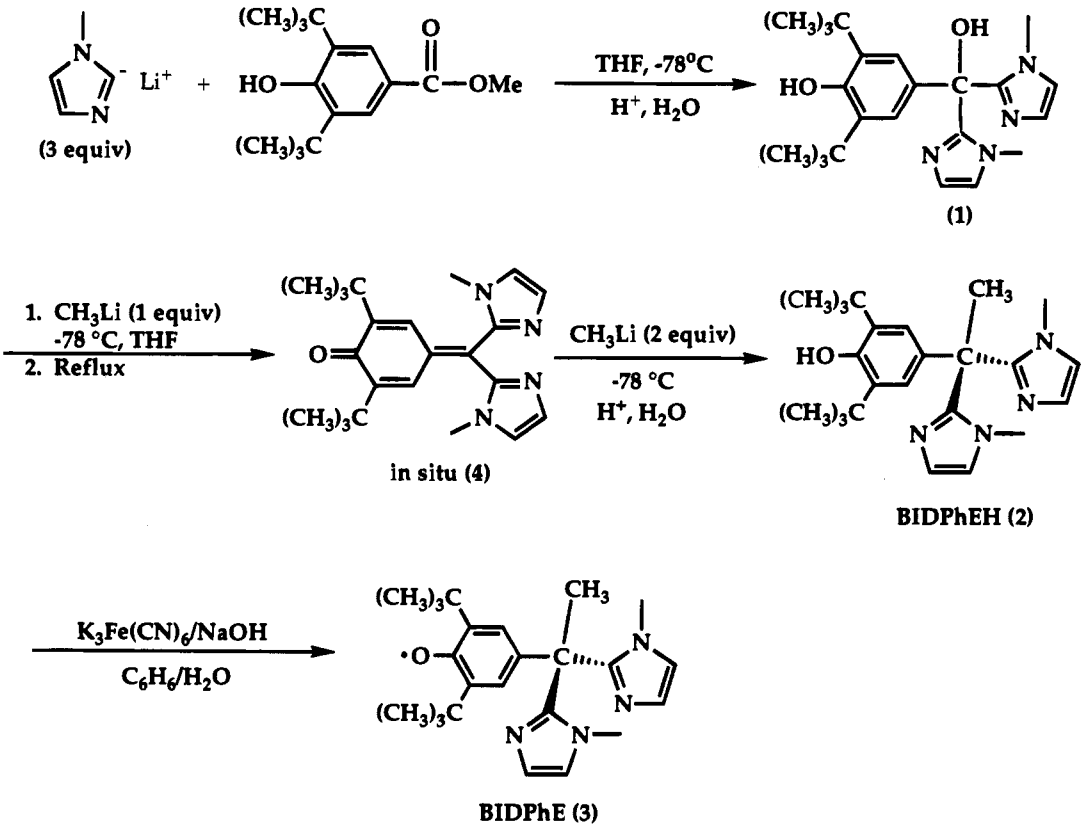

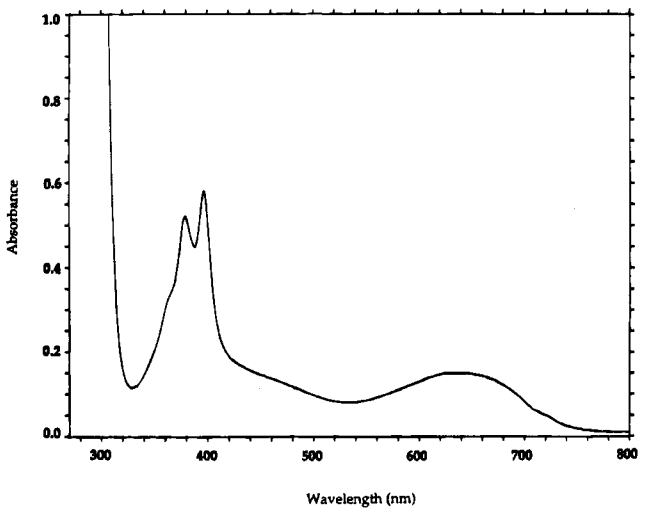

Figure 4. UV−visible absorption spectrum of BIDPhE (**3**) in CH_3CN.

The BIDPhEH ligand was designed to have quarternary carbon atoms at both ortho and para phenol ring positions. Such substituents are necessary to stabilize the phenoxyl radical against electron delocalization and ring coupling reactions.[55] Oxidation of phenols to the corresponding phenoxyl radicals can be accomplished by using various methods and oxidizing agents, including PbO_2 and $[Fe(CN)_6]^{3-}$.[56] The former reagent could oxidize **2** to the corresponding radical BIDPhE (**3**), but the conversion was never quantitative. Radical **3** proved to be stable to chromatography on silica gel plates, which always exhibited two major spots corresponding to the phenol starting material and radical product when PbO_2 was used as the oxidizing agent. The radical **3** is not stable to air over long periods (>1 h) in solution, and the chromatographic separation of **2** and **3** had to be carried out under strictly anaerobic conditions.

Use of potassium ferricyanide under basic conditions, as shown in Scheme 1, led to quantitative conversion of **2** to **3**. This procedure is more efficient than the PbO_2 method probably because the oxidizing agent is dissolved, rather than being suspended, in the reaction mixture and, more importantly, there is an excess of base present for removal of the phenolic proton. The radical **3** was isolated as a green solid simply by removing solvent from the organic layer. Although recrystallization of **3** can be accomplished from CH_2Cl_2 at −20 °C, this step causes a significant reduction in yield. Quantitation by chemical titration (see Experimental Section) revealed the radical content in **3** to be consistently >90%, making further purification steps unnecessary.

The UV−visible spectrum of a deep green solution of **3** in CH_3CN, shown in Figure 4, exhibits three distinct bands characteristic of substituted phenoxyl radicals.[55] The visible band at 638 nm proved to be useful in the characterization of the zinc complex $[Zn(BIDPhE)Cl_2]$, as well as the diferric complex **6**.[39] Radical **3** is stable in the solid state for ≥1 year if stored at −20 °C under anaerobic conditions, as monitored by the intensity of the 638 nm band.

The mononuclear complex $[Fe(BIDPhEH)_2Cl_2]^+$ was obtained by reaction of $FeCl_3$ with BIDPhEH. This complex was isolated with Cl^- as counterion (**5a**) when the ratio of BIDPhEH to iron employed was 2:1, and with $[FeCl_4]^-$ as counterion (**5b**) when a 1:1 ratio was used. An X-ray structure analysis of **5a** revealed the nature of the mononuclear complex, but was complicated by disorder problems. A structure of better quality was obtained with crystals of the $FeCl_4^-$ analogue **5b** and is discussed below.

(55) Altwicker, E. A. *Chem. Rev.* **1967**, *67*, 475−531.
(56) Thyagarajan, B. S. *Chem. Rev.* **1958**, *58*, 439−460.
(57) Tanase, T.; Watton, S. P.; Lippard, S. J. *J. Am. Chem. Soc.* **1994**, *116*, 9401−9402.
(58) Watton, S.; Davis, M. I.; Pence, L. E.; Rebek, J., Jr.; Lippard, S. J. *Inorg. Chim. Acta* **1995**, in press.

Scheme 2

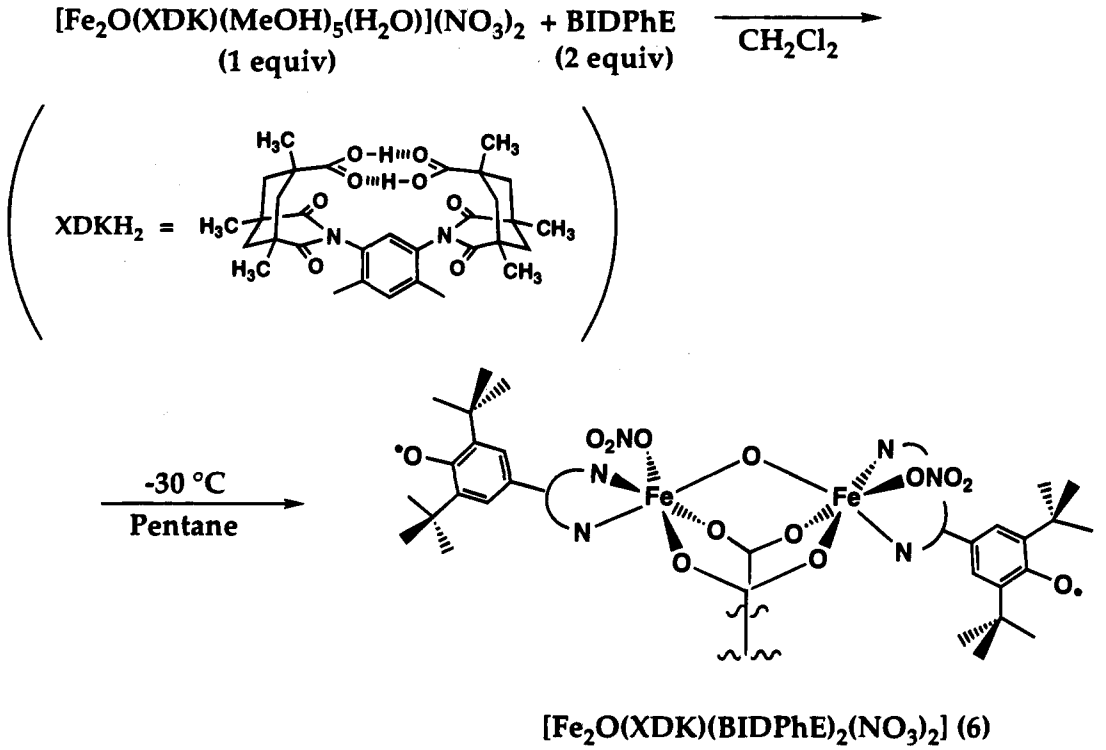

[Fe_2O(XDK)(BIDPhE)$_2$(NO_3)$_2$] (6)

Crystallization of **5b** typically occurred over a period of several weeks, making **5a** the more desirable compound for routine synthesis.

Attempts to prepare oxo, carboxylato-bridged diferric complexes with **2** or **3** as the capping ligand from ferric salts and simple carboxylates as starting materials[29] were unsuccessful. We therefore turned to the dinucleating ligand XDK (see Scheme 2). This preorganized, cleft-shaped bis(carboxylato) ligand has been developed in our laboratory as a general dinucleating ligand for use in the synthesis of a number of carboxylate-bridged diferric and heterodimetallic complexes.[30,57,58] The remarkably stable solvento complex [Fe_2O(XDK)(MeOH)$_5$(H_2O)](NO_3)$_2$, which is readily prepared in multigram quantities from $Fe(NO_3)_3$ and $XDKH_2$, has been used as a starting material for the preparation of several (μ-oxo)bis(μ-carboxylato)diiron(III) complexes with the bidentate nitrogen donor ligand 2,2′-dipyridyl (bpy), such as [Fe_2O(XDK)(bpy)$_2$(NO_3)$_2$], as well as the simple monodentate ligand 1-methylimidazole (1-MeIm).[30] These complexes are formed by substitution of the nitrogen donor ligands for the coordinated solvent molecules. This experience suggested that the solvento complex would be an excellent starting material for preparing the desired (μ-oxo)-bis(μ-carboxylato)diiron(III) complex with **3** as the capping ligand, provided that the radical could withstand the synthetic procedures.

Initial attempts to prepare **6** by combining **3** and the solvento complex in a variety of solvents, such as CH_3CN, THF, or MeOH, led to significant loss of radical content as judged by monitoring the 638 nm band in the UV−visible spectrum of the reaction mixture. Depending on the solvent employed, as much as 60% decay of the radical was noted 0.5 to 2.0 h after combination of the starting materials. When MeOH was employed, complete bleaching of the 638 nm band occurred immediately after addition of the solvento complex to a solution of **3**. Although the mechanism of this radical decomposition is presently unknown, a possible cause is reduction by the solvent, which in the case of MeOH would be accompanied by oxidation to form the aldehyde. Interestingly, the BIDPhE ligand alone shows little sign of decay after standing for several hours in MeOH. Oxidation of MeOH to formaldehyde has been implicated in the mechanism of the tyrosyl radical/cupric-containing enzyme galactose oxidase, as discussed elsewhere.[1]

Reaction of **3** with the solvento complex in CH_2Cl_2 gave mixtures in which the radical band at 638 nm showed no decay for several hours at room temperature, making this solvent the best candidate for crystallization of the desired product. The synthesis of [Fe_2O(XDK)(BIDPhE)$_2$(NO_3)$_2$] (**6**) is summarized in Scheme 2. Compound **6** was isolated as a crystalline solid from CH_2Cl_2/pentane mixtures at −30 to −40 °C. Spectroscopic characterization of **6**, including resonance Raman data reported elsewhere,[39] confirmed the presence of the noncoordinated phenoxyl radical of ligand **3** as well as the bent oxo-bridged diferric core. All of the data, including magnetic susceptibility and EPR measurements (vide infra), are consistent with the structure of **6** depicted in Scheme 2. This structure is analogous to that of crystallographically characterized compounds having bpy or 1-MeIm in place of BIDPhE in the external coordination sites.[30]

Molecular Structure of 5. As shown in Figure 2, compound **5** is a mononuclear ferric complex with two cis BIDPhEH ligands coordinated through the two imidazole nitrogen atoms, and two chloride ligands completing the coordination sphere. The overall geometry is approximately octahedral, as indicated by the angles reported in Table 2. Despite the preference of Fe(III) for oxygen-donor ligands, the bulky *tert*-butyl groups prevent coordination of BIDPhEH through its phenolic oxygen atom, as anticipated in the design of this ligand. The phenolic group is held pendant to the metal center, with an average Fe···O distance of 8.80(9) Å. This value is of interest to compare with that extracted from the saturation−recovery EPR experiments on compound **6** (vide infra).

The phenoxyl radical form of the ligand, BIDPhE, is expected to bind in the same manner. Conversion of the pendant phenol to a phenoxyl radical should not affect the chelating properties of the imidazole donor groups, since there is no pathway for delocalization of radical spin density onto the imidazole rings.

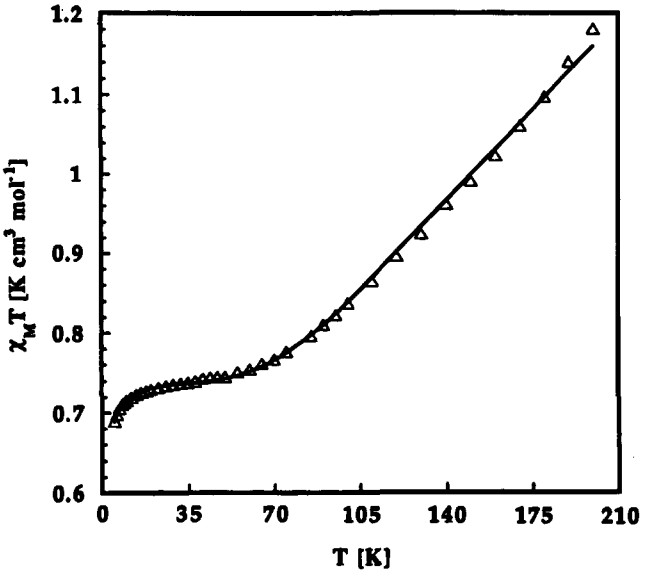

Figure 5. Plot of the molar susceptibility times temperature versus temperature for $[Fe_2O(XDK)(BIDPhE)_2(NO_3)_2]$ (**6**). The solid line represents the best fit by using the model given in eq 1, with $J = -117.5(4)$ cm^{-1} and $\theta = -0.47(2)$ K.

Comparison of the properties of the radical and non-radical analogues of the mononuclear zinc complexes [Zn(BIDPhEH)-Cl_2] and [Zn(BIDPhE)Cl_2] confirmed that BIDPhE and BIDPhEH coordinate in a similar fashion to Zn(II),[39] lending support to the conclusion that BIDPhE and BIDPhEH bind iron in the same fashion.

Magnetic Susceptibility Study of 6. A plot of the temperature dependence of χT for **6** is shown in Figure 5. The decrease in χT with decreasing temperature is characteristic of antiferromagnetic exchange coupling. Such behavior is expected for a (μ-oxo)bis(μ-carboxylato)diiron(III) compound, in which the coupling between two d^5 ($S = {}^5/_2$) iron atoms gives rise to an $S = 0$ ground state.[23] As the temperature is lowered, χT decreases until 40 K, at which temperature a plateau is observed. This plateau corresponds to the residual paramagnetism arising from the two $S = {}^1/_2$ radical ligands, which are uncoupled and exhibit Curie behavior. The theoretical value expected for the χT product of two such uncoupled spins is 0.75 cm^3 mol^{-1} K, assuming $g = 2.00$. The plateau in the χT curve for **6** occurs near 0.74 cm^3 mol^{-1} K, very close to the expected theoretical value. The downturn in χT at very low temperatures may be due to a small amount of radical–radical antiferromagnetic exchange, either between neighboring molecules or within the same diiron complex.

The susceptibility data were fit by least squares[59] to the theoretical model shown in eq 1, where $P = 2\exp(2J/kT) + 10\exp(6J/kT) + 28\exp(12J/kT) + 110\exp(30J/kT)$; $Q = 1 + 3\exp(2J/kT) + 5\exp(6J/kT) + 7\exp(12J/kT) + 9\exp(20J/kT) + 11\exp(30J/kT)$; $\chi_{imp} = (Ng^2\mu_B{}^2/3kT)(S(S+1))$ with $g = 2.00$ and $S = {}^5/_2$; IMP is a mole percentage of an $S = {}^5/_2$ impurity; TIP = temperature independent paramagnetism; $C_{rad} = (Ng_{rad}{}^2\mu_B{}^2/3k)(S(S+1))$; θ_{rad} = Weiss constant; g_{Fe} is the overall isotropic g value for the diiron center; g_{rad} is the overall isotropic g value for the radicals; and the other symbols have their usual meaning. This model includes the familiar expression derived from the Heisenberg isotropic spin exchange Hamiltonian for a dinuclear system, $\mathcal{H} = -2J \cdot S_1 \cdot S_2$, as well as a term that takes into account the uncoupled, Curie–Weiss behavior of the two $S = {}^1/_2$ radical sites.

$$\chi_M = \chi_{imp}(IMP) + (1\text{-}IMP)((2Ng_{Fe}{}^2\mu_B{}^2/kT)(P/Q)) + TIP + 2(C_{rad}/(T - \theta_{rad})) \quad (1)$$

The best fit to the data at all temperatures, shown in Figure 5, had only two parameters refined, the J value and the Weiss constant θ_{rad}. Both g values were fixed at 2.00, and IMP and TIP terms were fixed at zero. The refined values were $J = -117.5(4)$ cm^{-1} and $\theta = -0.47(2)$ K. A good fit was also obtained by refining g_{Fe} and g_{rad} along with J and θ, resulting in $J = -124(2)$ cm^{-1}, $\theta = -0.46(3)$ K, $g_{rad} = 2.00$, and $g_{Fe} = 2.11$. The overall g value for the diferric center in this latter fit is somewhat high compared to the expected value of $g = 2.00$ for a high-spin d^5 ion, and the fit was only marginally improved. If θ_{rad} was fixed at zero, the data above 25 K were fit well with J values near -120 cm^{-1}, but the theoretical χT product exhibited a plateau close to 0.75 cm^3 mol^{-1} K between 5 and 25 K, and gave a poor fit to the downturn in the experimental curve at low temperatures. The only way in which the downturn in the experimental χT product could be fit successfully was by the inclusion of a small negative θ_{rad} term, suggesting a small amount of interradical antiferromagnetic coupling, either intra- or intermolecular, in the low temperature regime. An excellent fit was also obtained if the data below 35 K were excluded and only the J value was refined, resulting in $J = -118.2(6)$ cm^{-1}, with both g values fixed at 2.00 and all other parameters set to zero. These results clearly indicate a J value of ca. -118 cm^{-1} for the antiferromagnetic exchange coupling constant, a value consistent with those determined for a variety of other (μ-oxo)bis(μ-carboxylato)diiron(III) complexes.[60,61] From this value and a previously reported correlation of iron–oxo bond length with J,[62] we predict a Fe–O oxo bridge distance of 1.78 Å.

The temperature-dependent magnetic behavior of the model complex **6** is strikingly similar to that exhibited by the tyrosyl radical/diferric form of the R2 protein of ribonucleotide reductase, for which a recent magnetic susceptibility study has been conducted.[63] The χT product for the protein also shows the characteristic decrease with decreasing temperature in the range 200–50 K for an antiferromagnetically coupled diferric core, followed by a plateau region at $T < 50$ K. In this case the plateau occurs at ca. 0.45 cm^3 mol^{-1} K, approximately half the plateau value for compound **6**, because there is only one radical per diiron unit in the protein active site. A least-squares fit of the data resulted in $J = -84(5)$ cm^{-1} for the (μ-oxo)(μ-carboxylato)diferric site in the protein.[63] This value may indicate hydrogen bonding to the oxo bridge.

EPR studies. Saturation–recovery EPR spectroscopy has recently been used[64,65] to probe the spin–lattice relaxation behavior of the tyrosyl radical (Tyr 122) in ribonucleotide reductase isolated from different sources. The rapid increase in the spin–lattice relaxation rate above ca. 20 K and the non-single exponential behavior of the saturation–recovery transients obtained at the higher temperature regime were attributed to the onset of a spin–lattice relaxation enhancement mechanism through the pairwise interaction of the tyrosyl radical, a slow-relaxing spin, with the neighboring diferric center, a fast-relaxing

(59) Vef, A. *Model2—Fit and Evaluation Program*; Institut für Anorganische Chemie und Analytische Chemie, Johannes-Gutenberg-Universität Mainz, 1989.

(60) Que, L., Jr.; True, A. E. *Prog. Inorg. Chem.* **1990**, *38*, 97–200.
(61) Kurtz, D. M., Jr. *Chem. Rev.* **1990**, *90*, 585–606.
(62) Gorun, S. M.; Lippard, S. J. *Inorg. Chem.* **1990**, *30*, 1625–1630.
(63) Atta, M.; Scheer, C.; Fries, P. H.; Fontecave, M.; Latour, J.-M. *Angew. Chem., Int. Ed. Engl.* **1992**, *31*, 1513–1515.
(64) Hirsh, D. J.; Beck, W. F.; Lynch, J. B.; Que L., J.; Brudvig, G. W. *J. Am. Chem. Soc.* **1992**, *114*, 7475–7481.
(65) Galli, C.; Atta, M.; Andersson, K. K.; Gräslund, A.; Brudvig, G. W. *J. Am. Chem. Soc.* **1995**, *117*, 740–746.

spin. The latter is rendered paramagnetic by population of its first excited spin state ($S = 1$) as the temperature is raised to 20 K. Two major contributions to the spin–lattice relaxation rate of the observed slowly relaxing spin can be discerned: (i) an isotropic term, denoted as $k_{1\text{scalar}}$, incorporating the intrinsic relaxation rate of the species (k_{1i}) and the relaxation arising from its exchange coupling (k_{1ex}) through spatial orbital overlap with a neighboring paramagnet; and (ii) an orientation-dependent term, $k_{1\theta}$, arising from the dipole–dipole interaction between the two paramagnets. The random orientation of the interspin vector relative to the applied magnetic field, applicable in the case of a non-oriented protein or an inorganic complex in a frozen glass, results in an angular distribution of the spin–lattice relaxation rates and gives rise to non-single exponential relaxation kinetics. Taking this fact into account, the saturation–recovery EPR transients can be fit by using eq 2, where

$$I(t) = 1 - N\int_0^{\pi} \sin\theta \cdot (\exp(-\{k_{1\text{scalar}} + k_{1\theta}\})t)\, d\theta \quad (2)$$

$I(t)$ is the intensity of the transient at time t, N is an adjustable scaling factor, $k_{1\text{scalar}} = k_{1i} + k_{1ex}$, and $k_{1\theta}$ is expressed by eqs 3 and 4 below.

As shown elsewhere,[64] for the case of a dipolar interaction between the tyrosyl radical in RR and the neighboring dinuclear ferric center, the "B" term of the dipolar alphabet is the dominant term in the theoretical expression for $k_{1\theta}$, which is then simplified as indicated by eq 3:

$$k_{1\theta} = k_{1d}^{B} \cdot (1 - 3\cos^2\theta)^2 \quad (3)$$

where

$$k_{1d}^{B} = \frac{\gamma_s^2 \mu_f^2}{6r^6} \frac{1}{\omega_s^2 (1 - g_f/g_s)^2 T_{2f}} \quad (4)$$

In eq 4, r is the interspin distance, γ_s, ω_s, and g_s are the magnetogyric ratio, the Larmor frequency, and the g value of the slow relaxer, respectively, and μ_f, T_{2f}, and g_f are the effective magnetic moment, the transverse (spin-spin) relaxation time and the g value of the fast relaxer, respectively. The "dipolar"-model fit to the saturation-recovery EPR transients with the use of eq 2 affords two rate constants, $k_{1\text{scalar}}$ and k_{1d}^{B}. The expression for μ_f for an antiferromagnetically coupled dinuclear ferric center is given by eq 5, if we assume that only the $S = 0$ and 1 spin states are significantly populated and by using $\mathcal{H}$

$$\mu_f^2 = g_f^2 (6 \exp(2J_{ex}/kT)) \quad (5)$$

$= -2J_{ex} \cdot S_1 \cdot S_2$ as the Heisenberg exchange Hamiltonian, where J_{ex} is the exchange coupling constant of the dinuclear center and k is the Boltzmann constant. In the case where only μ_f is temperature dependent, eqs 4 and 5 predict that a plot of $\ln(k_{1d}^{B})$ vs $1/T$ will be linear and have a slope of $2J_{ex}/k$.

The insets in Figures 3 and 6 show the first-derivative CW EPR spectra of the phenoxyl radical **3** as observed in the mononuclear compound [Zn(BIDPhE)Cl_2] and in the diferric model compound **6**, respectively. The arrows point to the zero-crossing point ($g = 2.00$) of the first-derivative spectra, which were the field settings used in the saturation–recovery experiments. The structureless nature of both CW EPR signals denotes a lack of proton nuclear hyperfine interaction, which is expected given the presence of the quarternary carbon atoms in the ortho and para phenyl ring positions. The radicals also have the same peak-to-peak widths ($\Delta H_{pp} \approx 9$ G), and the data

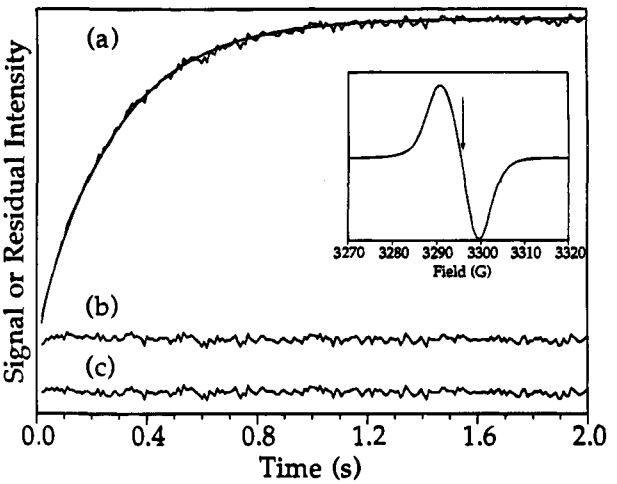

Figure 6. (a) Saturation–recovery EPR transient obtained for the BIDPhE radical in compound **6** (radical concentration 2 mM) at 6.7 K with a single-exponential fit superimposed. The observing microwave power was 0.29 μW, the saturating microwave power was 360 mW, and the pulse was of 600 ms duration. (b) Residual for the single-exponential fit. (c) Residual for the dipolar-model fit (eqs 2–3). Inset: Continuous-wave, X-band first derivative EPR spectrum of the BIDPhE radical in compound **6**. The arrow points to the zero-crossing point, used as the field position setting in the saturation–recovery experiment. Experimental conditions for the CW spectrum were the following: temperature 11.2 K; microwave frequency, 9.07 GHz; field-modulation amplitude, 4.0 G; microwave power, 0.72 μW; field-modulation frequency, 100 kHz.

are fully consistent with the fact that the CW signals arise from identical radical sources.

The intrinsic spin–lattice relaxation rate ($k_{1i} = 1/T_1$) of the phenoxyl radical BIDPhE (**3**) was measured by saturation–recovery EPR experiments on [Zn(BIDPhE)Cl_2]. Since Zn(II) is diamagnetic, the phenoxyl radical is expected to exhibit only its intrinsic relaxation, and consequently the saturation–recovery transients should show single-exponential behavior. A typical transient of the phenoxyl radical, obtained at 9.0 K, is shown in Figure 3a. It is single exponential in nature as clearly shown from the superimposed single-exponential fit and the quality of the residual. The residual obtained by using the dipolar model fit (Figure 3c) is identical with the one of the single exponential fit (Figure 3b), providing additional evidence that one adjustable parameter, $1/T_1$, is sufficient to account satisfactorily for the experimental data. The temperature dependence of the intrinsic relaxation rate of the phenoxyl radical is shown in Figure 7 (cross symbols) and it follows an $\approx T^{2.5}$ dependence. This dependence is very similar to that observed recently for other organic radicals.[66]

The spin–lattice relaxation behavior of the BIDPhE radical in the dinuclear Fe(III) compound (**6**) was examined in the temperature range 6.7–115 K. The saturation–recovery transients showed single exponential kinetic behavior in the range 6.7 K $< T <$ 70 K, which we denote as the "low" temperature regime. A typical experimental transient obtained at $T = 6.7$ K is shown in Figure 6a, with a single exponential fit superimposed. The temperature dependence ($k_{1i} = 1/T_1 \propto T^{2.5}$) and magnitude of the relaxation rate constants extracted from the single exponential fits are identical, within experimental error, to the ones of the radical in the [Zn(BIDPhE)Cl_2] compound, as clearly indicated in Figure 7 (open square and cross symbols). Thus, we conclude that any intraradical spin–spin exchange for **6**, either inter- or intramolecular in nature, is too small to enhance the intrinsic spin–lattice relaxation rate.

(66) Hirsh, D. J.; Brudvig, G. W. *J. Phys. Chem.* **1993**, *97*, 13216–13222.

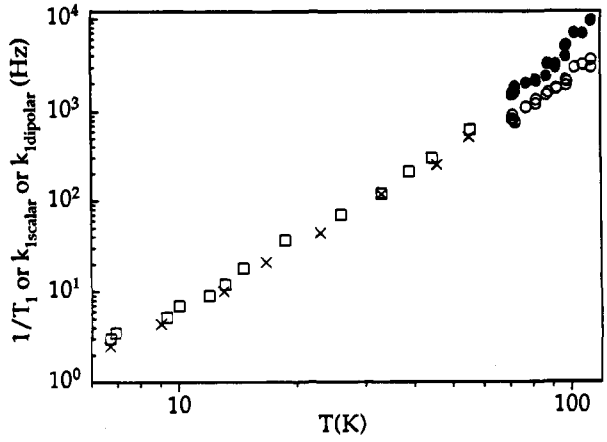

Figure 7. Temperature dependence of (a) the intrinsic spin–lattice relaxation rate ($1/T_1$) of the BIDPhE radical in the [Zn(BIDPhE)Cl_2] compound (×); (b) the intrinsic spin–lattice relaxation rate ($1/T_1$) of the BIDPhE radical in **6** (□); (c) the isotropic $k_{1scalar}$ rate constant of the BIDPhE radical in **6** (○); and (d) the dipolar rate constant, $k_{1dipolar}$ (≡ k_{1d}^B), of the BIDPhE radical in **6** (●). The $1/T_1$ values were extracted from single-exponential fits to the experimental traces. The values of $k_{1scalar}$ and $k_{1dipolar}$ were obtained from the dipolar-model fits to the non-single exponential saturation–recovery traces (eqs 2 and 3).

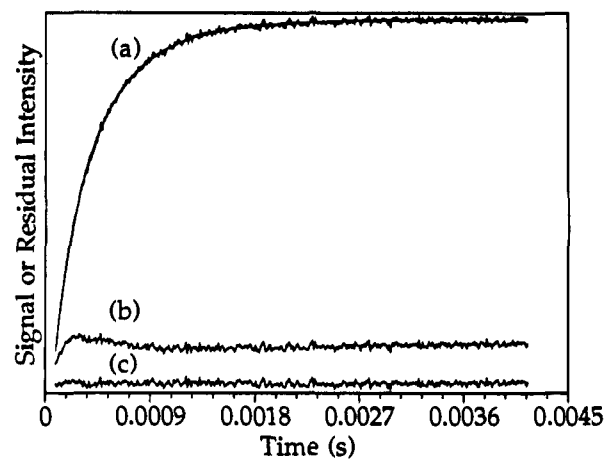

Figure 8. (a) Saturation-recovery EPR transient obtained for the BIDPhE radical in compound **6** (radical concentration 2 mM) at 87 K with a dipolar-model (eqs 2 and 3) fit superimposed. The observing microwave power was 2.87 μW, the saturating microwave power was 720 mW, and the pulse was of 1 ms duration. (b) Residual for the single-exponential fit. (c) Residual for the dipolar-model fit.

At temperatures above 70 K, the "high" temperature regime, the experimentally observed saturation-recovery traces of the phenoxyl radical in **6** exhibit non-single exponential kinetic behavior. A typical saturation–recovery curve obtained at 87 K is shown in Figure 8a, with a "dipolar" model fit superimposed. The fit provided by a single exponential is poor as judged from the residual shown in Figure 8b. This situation is reminiscent of the spin–lattice relaxation behavior of the Tyr122 radical in ribonucleotide reductase in its "high" temperature regime. In the present case, the population of the first excited spin state ($S = 1$) of the diferric center becomes significant above 70 K, making it a potent relaxation enhancer of the tethered phenoxyl radicals.

The scalar rate constants, $k_{1scalar}$, extracted from the B-term "dipolar" model fit (Figure 7, open circles, 72 K < T < 115 K) closely follow the magnitude and temperature dependence of the intrinsic relaxation rate of the phenoxyl radical as measured independently (Figure 7, open square and cross symbols). This behavior indicates that, in contrast to the case of ribonucleotide reductase, there is no significant exchange interaction due to spatial orbital overlap between the phenoxyl radical and the diferric center of **6**. One reason for this lack of overlap could be that a larger distance (≥10 Å) separates the two spin centers in **6** relative to the separation in ribonucleotide reductase, in which the distance between the tyrosyl (Tyr122) radical and the center of the diferric cluster, weighted for the spin density distribution on the phenyl ring, is ~7.7 Å.[65,67]

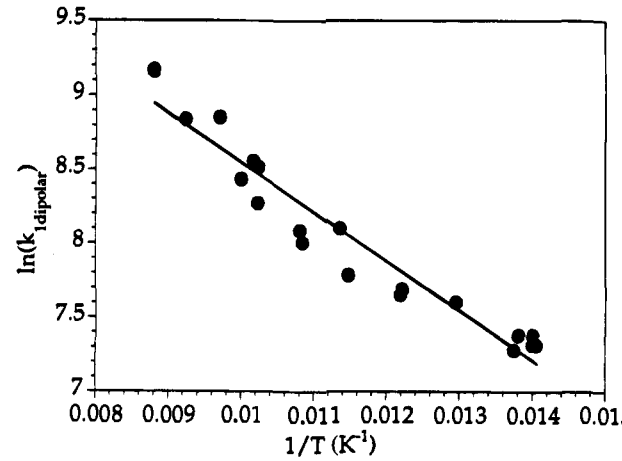

Figure 9. Natural logarithm of k_{1d}^B versus $1/T$ using the high temperature regime (72 K < T < 115 K) data of Figure 7. The linear fit corresponds to the equation $\ln(k_{1d}^B) = (11.8 \pm 0.3) + (333 \pm 21) \times (1/T)$.

The dipolar rate constants k_{1d}^B, extracted by using the B-term of the dipolar alphabet (Figure 7, full circles, 72 K < T < 115 K), exhibit an $\approx T^{4.0}$ temperature dependence, which is much steeper than the $\approx T^{2.5}$ dependence observed for the intrinsic relaxation rate of the radical at the "low" temperature regime (6.7 K < T < 70 K). It is important to note that the dipolar rate constants obtained are of identical magnitude, within experimental error, for radical concentrations between 0.2 and 2.0 mM, eliminating the possibility of intermolecular interactions playing any significant role in the observed relaxation enhancement effect.

Figure 9 shows a plot of $\ln(k_{1d}^B)$ vs $1/T$ for the data in the "high" temperature regime. As predicted from eq 5, the plot is linear and its slope gives $J_{ex} = (-115 \pm 7)$ cm^{-1} for the antiferromagnetic exchange coupling constant of the diferric center in **6**. This calculation is valid only if the transverse relaxation time, T_{2f}, of the diferric center is not temperature dependent. A series of arguments against a significant temperature dependence for T_{2f} have already been presented.[64] They also hold in the present case since we are studying a homologous pairwise dipolar interaction between phenoxyl radicals and a diferric center. In addition, the value for J_{ex} determined with the saturation–recovery EPR studies is in excellent agreement with the one determined independently through the magnetic susceptibility measurements. This result provides strong support for the use of the dipolar model to analyze the non-single exponential spin–lattice relaxation kinetics observed at T > 70 K for the phenoxyl radical in **6**. The ≈30 cm^{-1} larger value for the exchange coupling constant in **6** relative to *E. coli* ribonucleotide reductase R2 explains the higher temperature required to observe the onset of the dipolar relaxation enhancement of the radical in **6** relative to the protein (70 K vs 30 K).

Finally, it is possible to do a rough calculation of the average distance between the two paramagnets in **6**, the phenoxyl radical and the diferric center. The y-intercept of the expression for

(67) Hirsh, J. D. Ph.D. Thesis, Yale University, 1993.

$\ln(k_{1d}^{B})$ vs $1/T$ is given by $\ln[\gamma_s^2 g_f^2/\omega_s^2(1 - g_f^2/g_s^2)(T_{2f})r^6]$, which can be rewritten as $\ln(A/r^6)$, where the constant A incorporates all the terms dependent on γ_s, g_s, g_f, ω_s, and T_{2f}. The y-intercept values are 15.2 ± 0.2 and 11.8 ± 0.3 for *E. coli* R2 and **6**, respectively. Since in *E. coli* R2 we know that $r = 7.7$ Å, we can calculate the value of the constant A. By making the assumption that g_f, g_s, and T_{2f} are the same in both the protein and the model compound under study, we can make a rough estimate of 13.5 ± 1.2 Å for the average distance r between the phenoxyl radical and the diferric center in **6**.

This value has to be taken with caution since the assumption of identical g_f, g_s, and T_{2f} values for **6** and RR may not be valid. On the other hand, the fact that we do not observe any contribution to the spin−lattice relaxation from exchange between the radical and the diferric center indicates that they are located at least 10 Å apart,[68] a value which is in very good agreement with our rough estimate. In addition, we know that the phenolic oxygen atom to iron atom distance in **5b**, as well as the equivalent distance in the $[Zn(BIDPhE)Cl_2]$ compound, is ≈9 Å. We can then estimate that the distance from the phenolic oxygen atom to the center of the diferric cluster in **6** must be between 9 and 12.3 Å, given a typical Fe−Fe separation of 3.1−3.2 Å for (μ-oxo)bis(μ-carboxylato) complexes of this type.[30,60] The rough value of 13.5 ± 1.2 Å obtained for the interspin distance in **6** is in satisfactory agreement with all the experimental evidence.

Conclusions

The synthesis of a phenoxyl radical diiron complex (**6**) as a model for the active site in the R2 protein of ribonucleotide reductase has been accomplished by utilizing the dinucleating bis(carboxylato) ligand XDK, as well as the new stable phenoxyl radical ligand BIDPhE. Study of this compound by solid state magnetic susceptibility measurements and saturation−recovery EPR spectroscopy was facilitated by the fact that **6** could be obtained as a stable solid. Magnetic susceptibility measurements revealed temperature-dependent behavior that mimicked the protein data quite well, and could be fit by a simple spin exchange model that accounted for the presence of two $S = {}^1/_2$ radicals per diiron center and yielded a direct measure of the J value for the antiferromagnetic exchange in the $[Fe_2O(O_2CR)_2]^{2+}$ core.

The diiron model complex **6** and the mononuclear zinc complex $[Zn(BIDPhE)Cl_2]$ both give rise to identical singlets in their X-band CW EPR spectra, and these signals proved amenable to EPR saturation−recovery experiments. From fitting the saturation−recovery transients obtained over a range of temperatures to either a single-exponential model, as in the case of $[Zn(BIDPhE)Cl_2]$, or the dipolar model, as for **6**, both scalar and dipolar rate constants could be extracted. The zinc complex proved to be an excellent control compound for obtaining the intrinsic spin−lattice relaxation rate constant of the BIDPhE radical, and exhibited the temperature-dependent behavior expected for a simple organic radical. By comparison with the zinc complex, a clear rate enhancement for the BIDPhE radical in the diiron complex occurs in the high temperature range, fully consistent with the population of the first paramagnetic excited state of the nearby antiferromagnetically-coupled diiron center.

From a theoretical model of this behavior, the J value for the antiferromagnetic exchange coupling between the iron atoms in **6** was calculated to be -115 cm^{-1}, in remarkably good agreement with that obtained from the SQUID measurement, $J = -118$ cm^{-1}. The distance from the phenoxyl radical to the center of the diiron core was estimated to be 13.5 Å, also in good agreement with the value expected from an analysis of other structurally characterized diiron XDK complexes of this type and information obtained from the crystal structure of **5b**. Thus, all of the magnetic data on **6** are fully consistent with the proposed structure in Scheme 2. Both the magnetic susceptibility and spin saturation−recovery EPR techniques revealed overall behavior for the diiron model complex that was quite similar to that of the R2 active site and could distinguish important differences in parameters that were consistent with the structural differences between the model and the protein.

Acknowledgment. This work was supported by grants from the National Institute of General Medical Sciences (GM 32134 to S.J.L. and GM 36442 to G.W.B.).

Supplementary Material Available: Tables of complete atomic positional parameters, intramolecular bond distances and angles, and anisotropic thermal parameters for **5b** · CH_3CN (14 pages). This material is contained in many libraries on microfiche, immediately follows this article in the microfilm version of the journal, can be ordered from the ACS, and can be downloaded from the Internet; see any current masthead page for ordering information and Internet access instructions.

JA943780I

(68) Coffman, R. E.; Buettner, G. R. *J. Phys. Chem.* **1979**, *83*, 2387−2392.